Applied and Computational Harmonic Analysis 74 (2025) 101715

Contents lists available at ScienceDirect

Applied and Computational Harmonic Analysis

journal homepage: www.elsevier.com/locate/acha

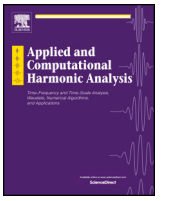

Full Length Article

# Unlimited sampling beyond modulo

Eyar Azar [a], Satish Mulleti [b,*], Yonina C. Eldar [a]

[a] Math and Computer Science, Weizmann Institute of Science, Rehovot, Israel
[b] Electrical Engineering, Indian Institute of Technology (IIT) Bombay, Mumbai, India

ARTICLE INFO

Communicated by Rayan Saab

*Keywords:*
Modulo sampling
Dynamic range
Shannon-Nyquist sampling
Unlimited sampling

ABSTRACT

Analog-to-digital converters (ADCs) act as a bridge between the analog and digital domains. Two important attributes of any ADC are sampling rate and its dynamic range. For bandlimited signals, the sampling should be above the Nyquist rate. It is also desired that the signals' dynamic range should be within that of the ADC's; otherwise, the signal will be clipped. Nonlinear operators such as modulo or companding can be used prior to sampling to avoid clipping. To recover the true signal from the samples of the nonlinear operator, either high sampling rates are required, or strict constraints on the nonlinear operations are imposed, both of which are not desirable in practice. In this paper, we propose a generalized flexible nonlinear operator which is sampling efficient. Moreover, by carefully choosing its parameters, clipping, modulo, and companding can be seen as special cases of it. We show that bandlimited signals are uniquely identified from the nonlinear samples of the proposed operator when sampled above the Nyquist rate. Furthermore, we propose a robust algorithm to recover the true signal from the nonlinear samples. Compared to the existing methods, our approach has a lower mean-squared error for a given sampling rate, noise level, and dynamic range. Our results lead to less constrained hardware design to address the dynamic range issues while operating at the lowest rate possible.

## 1. Introduction

Sampling plays a crucial role in representing analog signals digitally and processing them efficiently using digital signal processors. Among different sampling techniques, the Shannon-Nyquist sampling framework is widely used. In this framework, bandlimited signals are represented by their instantaneous samples with a sampling rate greater than or equal to the Nyquist rate, which is twice the maximum frequency component. The cost and power consumption of an analog-to-digital converter (ADC) increases with an increase in the sampling rate. Hence, it is desirable to sample the signals closer to the Nyquist rate.

Apart from the sampling rate, another key attribute of an ADC is its dynamic range. Ideally, the dynamic range of an ADC should be larger than that of the input analog signal; otherwise, the signal gets clipped. Clipping is a nonlinear process that results in loss of information. Several approaches have been proposed to address clipping or the dynamic range issue. These approaches can be broadly divided into two categories based on whether preprocessing is applied before sampling. One of the techniques that does not involve a preprocessing step uses the fact that samples of bandlimited signals are correlated when measured above the Nyquist rate. Such correlation among samples is used to retrieve any missing samples [1,2]. To address clipping, the signal is oversampled, and the clipped samples are considered as the missing ones, which are then recovered from the remaining unclipped samples. However,

* Corresponding author.
*E-mail address:* mulleti.satish@gmail.com (S. Mulleti).

https://doi.org/10.1016/j.acha.2024.101715
Received 26 February 2023; Received in revised form 24 July 2024; Accepted 2 October 2024

Available online 24 October 2024

theoretical guarantees are lacking for this approach. Specifically, identifiability results were not derived for estimating clipped samples from unclipped ones for bandlimited signals.

An alternative is to use spectral holes in the analog signal. The problem of clipping is prevalent in multiband communication systems where several signals are simultaneously transmitted [3,4]. This results in high-dynamic-range signals at the receiver and may result in clipping. Given its multiband nature, the received signal is assumed to have spectral holes. However, due to clipping, the received signal has wider bandwidth and does not have vacant bands. In [5,6], information about the vacant bands is used to differentiate between the original and clipped signals. In the aforementioned techniques, either large oversampling is required [1,2] or prior knowledge of the vacant bands is needed [5,6]. In addition, there are no theoretical guarantees derived for these approaches.

Clipping can be avoided by using an attenuator. In this approach, oversampling is not required. However, natural signals typically consist of a few large-amplitude regions and several regions with low amplitudes. Attenuation may push the low amplitude signals below the noise floor. Attenuators with variable gains, such as automatic gain controls (AGCs) and companders, are used in communication applications to address the dynamic range issue without distorting the small amplitude regions. In AGC, a chain of amplifiers is used with a feedback loop such that a suitable output level is maintained at the output [7,8]. The AGC circuit uses a closed-loop feedback mechanism, and maintaining circuit stability for different signal levels may be difficult.

Companding is an alternative, popular technique with variable gain where smaller amplitudes have larger gains compared to the larger ones. Companding is a nonlinear operation that increases the signal's bandwidth. Beurling proved that knowledge of the companded signal over the input signal's bandwidth is sufficient to uniquely identify the signal provided that the compander is a monotone function and its output to finite energy input has finite energy [9]. This result implies that a companded signal can be sampled at the Nyquist rate by applying an antialiasing filter before sampling. Landau et al. [10] proposed an iterative algorithm to recover a bandlimited signal from its companded and lowpass version. The algorithm converges to the true signal provided that the response of the compander is differentiable over the dynamic range of the input signal.

While the aforementioned companding-based methods operate at a minimal possible sampling rate, the requirement of monotonicity, differentiability, and finite energy output limits their hardware implementation [9], [10]. Specifically, it is difficult to realize a monotone operator over the entire signal's dynamic range. An additional approach to companding is to use a modulo operation before sampling to restrict the dynamic range. Specifically, the input signal is folded back when it crosses the dynamic range of the ADC. Hardware realization of such high-dynamic-range ADCs, also known as *self-reset* ADCs, are discussed in the context of imaging [11–14]. Along with samples of the modulo signal, these architectures store side information such as the amount of folding for each sample or the sign of the folding. Measuring the side information leads to complex circuitry at the sampler but enables computationally simple recovery.

Bhandari et al. considered *unlimited sampling*, where the side information is not measured and only folded or modulo samples are used for recovery [15]. The authors showed that for bandlimited signals sampling higher than the Nyquist rate is sufficient to identify the signal from its modulo samples uniquely. An algorithm to determine the true or unfolded samples from the modulo ones is suggested by applying an extension of Itoh's unwrapping method [16]. Specifically, the authors showed that by oversampling the bandlimited signals, there exists a positive integer $N$ such that the modulo of the $N$-th order differences of the modulo samples is equal to the $N$-th order differences of the true samples. Once the higher-order differences of the true samples are computed, the true samples are recovered by applying $N$-th order summation. The existence of such $N$ is guaranteed provided that the sampling rate is greater than or equal to $(2\pi e)$-times the Nyquist rate where $e$ is the Euler's constant. An oversampling factor (OF) 17 times is required [15]. In the presence of bounded noise, a much higher OF than $(2\pi e)$ is needed [15]. In addition, the recovery algorithm is sensitive to noise due to higher-order difference operations.

Romanov and Ordentlich [17] improved on the previous results and proposed an algorithm that requires the sampling rate to be slightly above the Nyquist rate. The authors leverage the fact that a time instant exists beyond which the signal lies within the dynamic range of the ADC. From these unfolded samples, the folded samples are predicted using the correlation among the samples. However, the simulation results of the algorithm are not presented, especially in the presence of noise. Multichannel extensions are considered in [18,19]. In the absence of noise, the authors in [18] showed that two channels, each of them operating at Nyquist rate, are sufficient to undo the modulo operation provided that the dynamic ranges of the two ADCs are coprime. The reconstruction is based on the application of the Chinese remainder theorem. Although perfect reconstruction is achieved by sampling at twice the Nyquist rate, the coprime requirement on the dynamic ranges of the ADCs limits its practical application. Modulo sampling is also extended to different problems and signal models such as periodic bandlimited signals [20], wavelets [21], a mixture of sinusoids [22], finite-rate-of-innovation signals [23], multi-dimensional signals [24], sparse vector recovery [25,26], the direction of arrival estimation problem [27], computed tomography [28], graph signals [29], neural recording [30], spike covariance estimation [31], and modulo hysteresis [32–34]. In addition to theory and algorithms, hardware prototypes of high-dynamic range ADCs by using modulo operators are presented in [20,35,36].

In summary, AGC, companding, and modulo are different ways of addressing the dynamic range issues. However, there are several drawbacks in the current literature, such as missing theoretical guarantees, stability, requirements of smooth and monotone operators, and algorithms operating at high sampling rates. In addition, the solutions are developed independently and lack common recovery methods. A single reconstruction algorithm that can robustly recover bandlimited signals from clipped, companded, or modulo samples in the presence of noise and from the minimal sampling rate is lacking.

In this paper, we present a general framework to address the dynamic range issues of the ADCs, where all existing approaches can be treated as special cases and provide scope for designing new amplitude limiters. Specifically, we consider a non-linear transformation function before sampling with the following desired response to a bandlimited input signal: (a) if the input signal is within the dynamic range of the ADC, then the response remains within the dynamic range and should be invertible; (b) for the part of the

input signal beyond the dynamic range of the ADC, the output can take any arbitrary values. Invariability within the dynamic range of the ADC aids in achieving companding with any desired response and uniqueness when recovering the actual samples from the non-linear samples. We then propose a sampling efficient and robust algorithm to recover the signal. Our algorithm uses the fact that the residual signal, the difference between the true signal and the output of the nonlinear operator, is time-limited for bandlimited signals. Hence, one can differentiate between the input signal and the residue beyond the signal's bandwidth. By oversampling the output of the nonlinear operator, we present an approach to recover the residual signal from the nonlinear samples. With this brief introduction, we summarize our main contributions in the following.

- We propose a non-linear operator that restricts a signal's dynamic range to a desired limit.
- The proposed operator is generalized, including clipping, modulo, commanding, and more.
- We derive theoretical guarantees and show that sampling above the Nyquist rate is necessary and sufficient to recover the samples.
- Due to the generality of the operator, these guarantees apply to clipping (which were missing in previous works) and companding as well. Further, for companding, we do not require any smoothness constraints as in previous results, and hence, a wider class of companders can be used.
- For companding, we do not require any smoothness constraints as in previous results, and hence, a wider class of companders can be used.
- We proposed an algorithm beyond bandwidth residual reconstruction to determine the true samples from the folded ones.
- In its simplest form, the algorithm could be implemented by using a matrix inversion for a small-scale problem.
- We propose a noise-robust algorithm for a large-scale problem using a projected sub-gradient method.
- We show that the proposed algorithm can reconstruct signals from non-linearities such as clipping, modulo operation, and commanding. We are unaware of previous algorithms that can recover samples for such a wide variety of non-linearities.
- We compare our algorithm for modulo operation with those in [15] and [17]. We show that our method reconstructs the signal for a given noise level and dynamic range of the ADC for a lower sampling rate in comparison with existing approaches and with smaller errors.

The paper is organized as follows. In Section 2, we define the class of generalized, non-linear operators considered in this paper and present the problem formulation. Identifiability results are derived in Section 3. In Section 4, we present the proposed algorithm. Simulation results are provided in Section 5 followed by conclusions.

We use the following notations and definitions in the paper. For a continuous-time analog signal $f(t)$, its Fourier transform is denoted as $F(\omega)$. Uniform samples of $f(t)$ are denoted by $f(nT_s)$ where $T_s > 0$ is the sampling interval and $n \in \mathbb{Z}$. The corresponding sampling rate is $\omega_s = \frac{2\pi}{T_s}$ rads/sec. For a sequence $f(nT_s)$ its corresponding boldfaced symbol $\mathbf{f}$ denotes its vector form with $n$-th entry $\mathbf{f}[n] = f(nT_s)$. The discrete-time Fourier transform (DTFT) is defined as

$$\mathcal{F}\mathbf{f} = F(e^{\mathrm{j}\omega T_s}) = \sum_{n\in\mathbb{Z}} f(nT_s)\, e^{-\mathrm{j}\omega n T_s}. \tag{1}$$

For any interval $\rho \subset (-\omega_s/2, \omega_s/2)$, $\mathcal{F}_\rho\mathbf{f}$ denotes a partial DTFT $F(e^{\mathrm{j}\omega T_s})$ evaluated over $\omega \in \rho$, and $\mathcal{F}_\rho^*$ denotes the adjoint operator of $\mathcal{F}_\rho$. Specifically, we have

$$\mathcal{F}_\rho^*\mathcal{F}\mathbf{f}[n] = \frac{T_s}{2\pi}\int_\rho F(e^{\mathrm{j}\omega T_s})\, e^{\mathrm{j}\omega n T_s}\,\mathrm{d}\omega, \quad n \in \mathbb{Z}. \tag{2}$$

For any integer $N$, $\mathcal{S}_N$ denotes the space of sequences that have support over $\{-N, \cdots, N\}$, and $P_{\mathcal{S}_N}$ denotes the orthogonal projection onto the space $\mathcal{S}_N$ which sets all samples beyond $\{-N, \cdots, N\}$ to zero. The indicator function on domain $\mathcal{A}$ is denoted by $\mathbf{1}_{\mathcal{A}}(\cdot)$. The symbol $\mathrm{B}_{\omega_m}$ denotes the space of analog signals that are bandlimited to frequency interval $[-\omega_m, \omega_m]$. The sinc function is defined as $\mathrm{sinc}(x) = \frac{\sin(\pi x)}{\pi x}$. For any two functions $g(t)$ and $f(t)$, a composite function is denoted as $g \circ f(t)$. For any $a \in \mathbb{R}$ and $\lambda \in \mathbb{R}^+$, the modulo operation $\mathcal{M}_\lambda(\cdot)$ is given as

$$\mathcal{M}_\lambda(a) = (a + \lambda) \bmod 2\lambda - \lambda. \tag{3}$$

## 2. Problem statement

### 2.1. Preliminaries

Consider a signal $f(t) \in \mathrm{B}_{\omega_m}$, an ADC with dynamic range $[-\lambda, \lambda]$, and sampling interval $T_s$. If the uniform samples $f(nT_s)$ are beyond the dynamic range of the ADC, then they are clipped. Specifically, the output samples of the ADC $f_\lambda(nT_s)$ are given as

$$f_\lambda(nT_s) = \begin{cases} -\lambda, & f(nT_s) \le -\lambda, \\ f(nT_s), & |f(nT_s)| < \lambda, \\ \lambda, & f(nT_s) \ge \lambda. \end{cases} \tag{4}$$

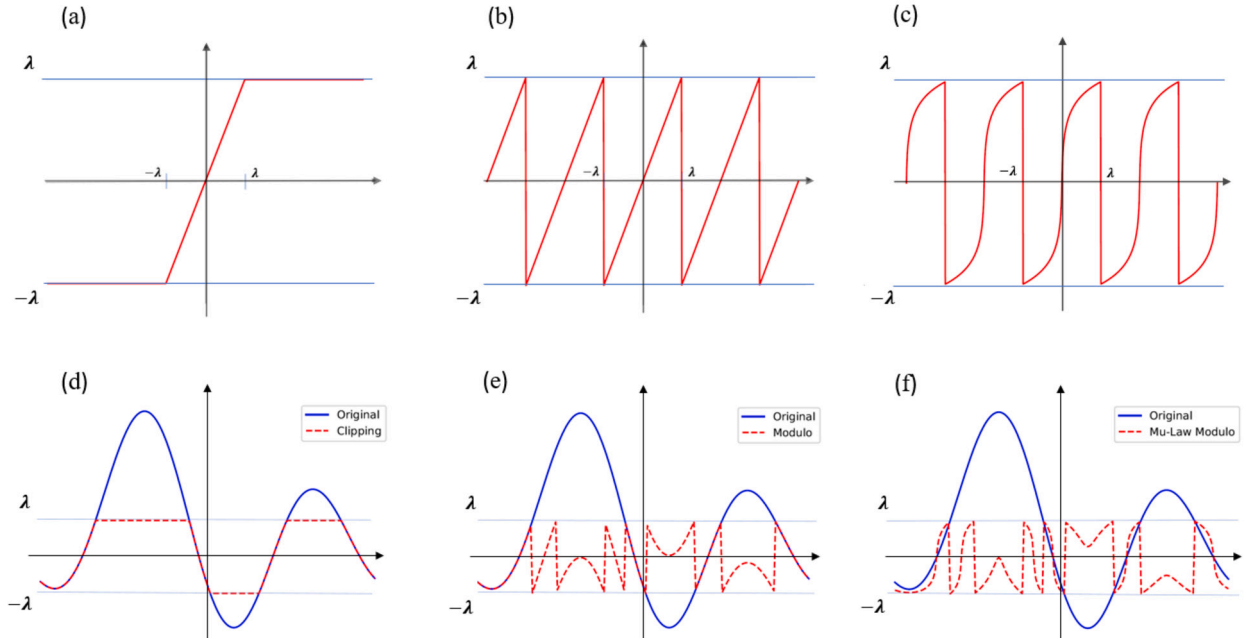


**Fig. 1.** Examples of three non-linear functions:(a) Clipping as in (4) (b) $\lambda$-modulo (c) $\mu$-law modulo (d) A bandlimited signal and its clipped version; (e) A bandlimited signal and output of modulo nonlinear operator; and (f) A bandlimited signal and output of a $\mu$-law modulo operator.

Clipping results in loss of information and generally requires a high amount of oversampling to estimate $f(nT_s)$ from $f_\lambda(nT_s)$ for all $n \in \mathbb{Z}$ [1,2]. To avoid clipping, instantaneous companding or modulo operations are used before sampling, limiting the signal's dynamic range. Instantaneous companding uses a nonlinear, monotone function $\mathcal{G} : \mathbb{R} \to \mathbb{R}$ such that $\mathcal{G}f(t) \in [-\lambda, \lambda]$ [9]. One can recover $f(nT_s)$ from $\mathcal{G}f(nT_s)$ by sampling at or above the Nyquist rate. In addition, $\mathcal{G}$ boosts low amplitudes of the signal to improve the signal-to-noise ratio (SNR), which helps in accurate recovery. Existing companders are required to be monotone, differentiable, and $\mathcal{G}f(t) \in L^2(\mathbb{R})$ which limits their practical application [9,10]. An alternative to avoid clipping is to perform a modulo operation prior to sampling, that is, sample $\mathcal{M}_\lambda f(t)$ instead of $f(t)$ [15]. As in companding we have that $\mathcal{M}_\lambda f(t) \in [-\lambda, \lambda]$. The existing algorithms to determine $f(nT_s)$ from $\mathcal{M}_\lambda f(nT_s)$, either operate at very high sampling rate [15] or result in large reconstruction error in the presence of noise as discussed later in the simulation section.

Our objective is to devise a non-linear operation that has advantages over existing approaches, such as companding and modulo, and the existence of a robust, practical recovery algorithm that operates at a rate closer to the Nyquist rate. To this end, we consider the following non-linear operator:

$$\mathcal{G}_\lambda f(t) = \begin{cases} \text{arbitrary}, & |f(t)| > \lambda, \\ g \circ f(t), & |f(t)| \le \lambda, \end{cases} \tag{5}$$

where $g : [-\lambda, \lambda] \to [-\lambda, \lambda]$ is a known, continuous, and invertible function. As we show later, our recovery does not depend on the response of the nonlinear operator for $|f(t)| > \lambda$, and hence we chose an arbitrary response.

Both clipping and modulo operators are special cases of the operator $\mathcal{G}_\lambda$. To illustrate this, three examples of $\mathcal{G}_\lambda$ are demonstrated in Fig. 1 together with their responses to a bandlimited signal. Fig. 1(a) and Fig. 1(b) illustrate the output of clipping (cf (4)) and modulo $\mathcal{M}_\lambda$, respectively. In these two special cases, the function $g(t)$ is identity, that is, $g \circ f(t) = f(t)$, for $|f(t)| \le \lambda$. For $|f(t)| > \lambda$, $\mathcal{G}_\lambda f(t) = \text{sgn}(f(t))\,\lambda$ for clipping and $\mathcal{G}_\lambda f(t) = \mathcal{M}_\lambda f(t)$ for modulo. Their outputs to a bandlimited signal are displayed in Fig. 1(d) and Fig. 1(e). Fig. 1(c) shows that the output of an operator consists of a $\mu$-law operator[1] followed by modulo operations. Its output to a bandlimited signal is exhibited in Fig. 1(f), where amplitudes closer to zero are amplified. Both clipping and modulo operation are well-known in the literature. However, the $\mu$-law modulo operator is a novel one, which is a combination of compander and modulo operators. These examples demonstrate that by careful selection of $g(t)$ and the response of the operator for $|f(t)| > \lambda$, different non-linear functions could be realized. In addition, it can be shown that companders, such as $\mu$-law and $A$-law, are special cases of the generalized operator.

[1] A $\mu$-law operator is used for companding. Its response to a function $f(t)$ is $\text{sgn}(f(t))\dfrac{\ln\left(1+\mu|f(t)|/\|f(t)\|_\infty\right)}{\ln(1+\mu)}$ where $\mu > 0$.

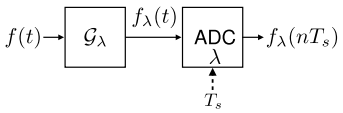


**Fig. 2.** A schematic of generalized sampling: The bandlimited signal $f(t)$ is processed through a non-linear operator $\mathcal{G}_\lambda$ and then sampled by the ADC with a sampling interval $T_s$. The dynamic range of the ADC is $[-\lambda, \lambda]$.

### 2.2. Problem formulation

Consider a bandlimited signal $f(t)$, non-linear operator, $\mathcal{G}_\lambda$, which operates on $f(t)$, and then sampled using an ADC with dynamic range $[-\lambda, \lambda]$ and sampling rate $\frac{1}{T_s}$. The overall sampling scheme is shown in Fig. 2. Since the ADC clips signals beyond its dynamic range, we can assume that the output of the operator is followed by a clipping operation prior to ADC. Hence, if we consider the response of the generalized operator together with the explicit clipping (due to ADC), we have that

$$|\mathcal{G}_\lambda f(t)| \leq \lambda. \tag{6}$$

In other words, the outcome of $G_\lambda f(t)$ is bounded to $[-\lambda, \lambda]$.

Our goal is to derive conditions on the sampling rate such that the signal $f(t)$ is uniquely identified from the *non-linear* or *folded* samples $f_\lambda(nT_s)$. Note that if one recovers the *unfolded* or *true* samples $f(nT_s)$ from $f_\lambda(nT_s)$ then $f(t)$ can be uniquely reconstructed from $f(nT_s)$ provided the sampling rate is greater than or equal to the Nyquist rate. In the rest of the discussion, we assume that there exist one or more samples such that $|f(nT_s)| > \lambda$. The assumption ensures that there are folded samples on which unfolding methods can be applied.

Non-linear operators prior to sampling, as shown in Fig. 2, are not new in the sampling literature. For example, Zhu [37] considers a non-linear sampling framework where an operator is used to convert an arbitrary signal to a bandlimited one. The framework enables the extension of the Shannon-Nyquist sampling framework to non-bandlimited functions. In another line of work, Dvorkind et al. [38] considered a non-linear operator together with a non-ideal sampling setup. The framework reflects the practical scenario where the measurement devices have inherent nonlinearities and may not be measuring exact instantaneous (or ideal) samples. The authors derive conditions on the non-linearity and input signal model for perfect recovery. In addition, practical algorithms for signal reconstruction were discussed. Unlike these earlier works [37,38], the operators considered in this work are not necessarily invertible.

In the next section, we derive identifiability results (which are independent of any recovery algorithm) for recovering bandlimited signals from samples of the non-linear operator. In Section 4, we present the proposed algorithms to recover the signal from minimal samples.

## 3. Theoretical guarantees

In this section, we derive necessary and sufficient conditions to uniquely identify a bandlimited function from its samples measured via the non-linear operator $\mathcal{G}_\lambda$.

Our main result is summarized in the following theorem.

**Theorem 1** *(Identifiability conditions). Consider the sampling scheme shown in Fig. 2 where the operator $\mathcal{G}_\lambda$ is defined as in (5). Then any signal $f(t) \in L^2(\mathbb{R}) \cap B_{\omega_m}$ is uniquely identifiable from its non-linear samples $\{f_\lambda(nT_s)\}$ iff sampling is performed above the Nyquist rate, that is, $T_s < \frac{\pi}{\omega_m}$.*

**Proof.** See Appendix A. □

Theorem 1 implies that it is necessary and sufficient to sample above the Nyquist rate to uniquely identify a bandlimited signal from the samples of the non-linear operator $\mathcal{G}_\lambda$. Since the modulo operator $\mathcal{M}_\lambda$ is a special case of $\mathcal{G}_\lambda$, the result holds true for the modulo operator. Particularly, in terms of sampling rate, our sufficiency results are similar to that in [15], and hence Theorem 1 is consistent with existing results. Note that, to the best of our knowledge, the necessary condition of sampling above the Nyquist rate has been proved for the first time in this work. Our identifiability result depends only on the samples of $g \circ f(t)$ and not on the measurements of $\mathcal{G}_\lambda f(t)$ for $|f(t)| > \lambda$.

The identifiability results are independent of any algorithm. In practice, unfolding algorithms may require operating at a much higher rate than the Nyquist rate.

Since both clipping and companding are particular instances of the proposed operator, the results also hold for them. Hence, theoretically, it is possible to recover the clipped samples if they are measured over the Nyquist rate. In the case of companding, unlike Beurling's results [9], our guarantees do not require the operator to be smooth and hence extend the results to a broader class of companders.

## 4. A robust and lowrate recovery algorithm

We next present an iterative algorithm for recovery of the samples $f(nT_s)$ from the non-linear samples $f_\lambda(nT_s) = \mathcal{G}_\lambda f(nT_s)$. The algorithm assumes that the sampling rate is greater than the Nyquist rate, that is, $\omega_s > 2\omega_m$. The underlying principle of the algorithm is to use the out-of-band energy of the non-linear samples to reconstruct the residual signal. The residual signal is the difference between the true signal and the non-linear one. For this reason, we refer to the proposed algorithm as *beyond bandwidth residual reconstruction ($B^2R^2$)*. For ease of discussion, we first present the method for the modulo operator and then extend it to the general non-linear operator. The modulo setting is also considered in [39].

### 4.1. $B^2R^2$ algorithm for modulo operator

For $\mathcal{G}_\lambda = \mathcal{M}_\lambda$, the modulo samples are expressed as a linear combination of the true samples and a residual signal:

$$f_\lambda(nT_s) = f(nT_s) + z(nT_s), \tag{7}$$

where values of the residual sequence $z(nT_s)$ are integer multiples of $2\lambda$. Our approach is to first compute $z(nT_s)$ from the modulo samples $f_\lambda(nT_s)$ and then use (7) to determine $f(nT_s)$. To derive $z(nT_s)$ from $f_\lambda(nT_s)$, we use the following two properties of the finite energy bandlimited signals to separate $f(nT_s)$ from $f_\lambda(nT_s)$.

- Time-domain separation [17]: From the Riemann-Lebesgue Lemma it can be shown that $\lim_{|t|\to\infty} f(t) = 0$. This implies that for any $\lambda > 0$ there exists an integer $N_\lambda$ such that $|f(nT_s)| < \lambda$, for all $|n| > N_\lambda$. Hence, for $|n| > N_\lambda$, we have $f_\lambda(nT_s) = f(nT_s)$ and $z(nT_s) = 0$. Thus, the modulo samples are equal to the true samples over a set of indices, and they are used to distinguish the residual from the modulo samples in time.
- Fourier-domain separation: Since the signal is sampled above the Nyquist rate,

$$F(e^{\mathrm{j}\omega T_s}) = 0, \quad \text{for} \quad \omega_m < |\omega| < \omega_s/2. \tag{8}$$

By using the linearity of DTFT, from (7) we have that

$$F_\lambda(e^{\mathrm{j}\omega T_s}) = Z(e^{\mathrm{j}\omega T_s}), \quad \text{for} \quad \omega_m < |\omega| < \omega_s/2. \tag{9}$$

This implies that one can differentiate the DTFT of the true samples and that of the residual by sampling above the Nyquist rate and looking beyond the bandwidth.

In the rest of the discussion, we assume that $N_\lambda$ is known. From the time-domain separation, we infer that the residual signal has finite support on the integer set $\mathcal{N}_\lambda = \{-N_\lambda, \cdots, N_\lambda\}$. Combining the time-domain and the frequency-domain separations, we arrive at the following relation:

$$F_\lambda(e^{\mathrm{j}\omega T_s}) = \sum_{n=-N_\lambda}^{N_\lambda} z(nT_s) e^{-\mathrm{j}nT_s\omega}, \tag{10}$$

for $\omega_m < |\omega| < \omega_s/2$. Due to its finite support, the DTFT of $z(nT_s)$ is a trigonometric polynomial and it is given over an interval.

#### 4.1.1. A simple matrix-inversion-based solution

From (10) one can determine $z(nT_s)$ by sampling $F_\lambda(e^{\mathrm{j}\omega T_s})$ at $2N_\lambda + 1$ points over the interval $\rho = (-\omega_s/2, -\omega_m) \cup (\omega_m, \omega_s/2)$ and inverting the resulting set of linear equations. The matrix that relates $z(nT_s)$ and samples of $F_\lambda(e^{\mathrm{j}\omega T_s})$ will have a Vandermonde structure with size $(2N_\lambda + 1) \times (2N_\lambda + 1)$. The Vandermonde matrix is invertible if the $2N_\lambda + 1$ points over the interval $\rho = (-\omega_s/2, -\omega_m) \cup (\omega_m, \omega_s/2)$ are unique. From the recovered residual signal, the true samples $f(nT_s)$ are determined by using (7). In principle, the approach is similar to the algorithm proposed in [20] for periodic bandlimited signals.

Although the proposed approach looks simple, the matrix inversion used for estimating $z(nT_s)$ from the samples of $F_\lambda(e^{\mathrm{j}\omega T_s})$ may be unstable for large values of $N_\lambda$. To illustrate this suppose that $f(t) = \mathrm{sinc}(t)$ where $\omega_m = 2\pi$. We consider its samples measured at a rate of $12\omega_m$, that is, with an oversampling factor of 6. We used a modulo operator to limit the dynamic range before sampling and reconstructing by Vandermonde matrix inversion for $\lambda = 0.25$ and $\lambda = 0.2$. The true signals and the reconstructed signals are shown in Fig. 3. For $\lambda = 0.25$, $N_\lambda = 4$ and we observe perfect reconstruction, whereas, for $\lambda = 0.2$, $N_\lambda = 9$ and perfect recovery is not achieved as shown in Fig. 3(b). In the following, we discuss an iterative algorithm that does not require matrix inversion and can reconstruct signals for larger values of $N_\lambda$.

#### 4.1.2. $B^2R^2$: an iterative, optimization-based, computationally efficient solution

Here, we propose an iterative algorithm that does not require any matrix inversion. The iterative algorithm is a solution to an optimization problem, as discussed below. By using the operator and vector notations, we rewrite (9) as

$$\mathcal{F}_\rho \mathbf{f}_\lambda = \mathcal{F}_\rho \mathbf{z}, \tag{11}$$

where $\rho = (-\omega_s/2, -\omega_m) \cup (\omega_m, \omega_s/2)$. Since $z(nT_s)$ is time-limited to $\mathcal{N}_\lambda$, we have that

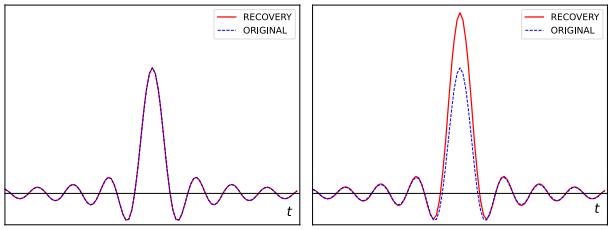


(a) $\lambda = 0.25, N_\lambda = 4$ (b) $\lambda = 0.20, N_\lambda = 9$

**Fig. 3.** Reconstruction of bandlimited signals from its modulo samples by using Vandermonde inverse: (a) Perfect reconstruction and (b) Imperfect recovery. As $N_\lambda$ increases, the matrix inversion becomes unstable, and perfect recovery is not achieved.

$$\mathbf{z} \in \mathcal{S}_{N_\lambda}. \tag{12}$$

Given the data-fitting term in (11) and support constraint, recovery of $\mathbf{z}$ can be written as the following optimization problem:

$$\min_{\mathbf{z}} \quad \mathrm{C}(\mathbf{z}) = \frac{1}{2}\|\mathcal{F}_\rho \mathbf{f}_\lambda - \mathcal{F}_\rho \mathbf{z}\|^2 \quad \text{s.t.} \quad \mathbf{z} \in \mathcal{S}_{N_\lambda}. \tag{13}$$

Problem (13) can be solved using a projected gradient descent (PGD) [40, Page 264] method where at each iteration, the solution iterates towards the negative gradient of the cost $\mathrm{C}(\mathbf{z})$ and is then projected onto the space $\mathcal{S}_{N_\lambda}$. In summary, starting from an initial point $\mathbf{z}^0 \in \mathcal{S}_{N_\lambda}$, the steps at the $k$-th iteration are

$$\begin{aligned} \mathbf{y}^k &= \mathbf{z}^{k-1} - \gamma_k \nabla \mathrm{C}(\mathbf{z}^{k-1}) \\ \mathbf{z}^k &= P_{\mathcal{S}_{N_\lambda}}(\mathbf{y}^k), \end{aligned} \tag{14}$$

where $\gamma > 0$ is a suitable step-size, $\nabla \mathrm{C}(\mathbf{z}) = \mathcal{F}_\rho^* \mathcal{F}_\rho(\mathbf{z} - \mathbf{f}_\lambda)$ is the gradient of $\mathrm{C}(\mathbf{z})$ and $P_{\mathcal{S}_{N_\lambda}}(\cdot)$ is the orthogonal projection onto $\mathcal{S}_{N_\lambda}$. The operator $\mathcal{F}_\rho^* \mathcal{F}_\rho$ is a highpass operation. The sequence $\mathcal{F}_\rho^* \mathcal{F}_\rho(\mathbf{z} - \mathbf{f}_\lambda)$ is computed by filtering the sequence $\mathbf{z} - \mathbf{f}_\lambda$ with an ideal highpass filter with spectral support over $\rho$. Both the steps (14) do not require matrix inversion and hence instability.

Additionally, one can note that the loss function, $C(\mathbf{z})$, is $1-$smooth function, that is, for $\mathbf{z}_1, \mathbf{z}_2$ it holds that $\|\nabla C(\mathbf{z}_1) - \nabla C(\mathbf{z}_2)\| < \|\mathbf{z}_1 - \mathbf{z}_2\|$. To prove this, we note that

$$\nabla C(\mathbf{z}) = \mathcal{F}_\rho^* \mathcal{F}_\rho(\mathbf{z} - \mathbf{u}).$$

Then we have

$$\|\nabla C(\mathbf{z}_1) - \nabla C(\mathbf{z}_2)\| \leq \|\mathcal{F}_\rho^* \mathcal{F}_\rho\| \, \|\mathbf{z}_1 - \mathbf{z}_2\| \leq \|\mathbf{z}_1 - \mathbf{z}_2\|.$$

Hence, since $C(\mathbf{z})$ is quadratic and $1-$smooth it yields that a projected gradient descent with step size $\gamma = 1$ satisfies [40, Page 267]

$$C(\mathbf{z}_k) - C(\mathbf{z}^*) \leq \frac{2\|\mathbf{z}_1 - \mathbf{z}^*\|}{k-1}.$$

In the case of modulo operation, the residual signal has an additional structure that every element of $\mathbf{z}$ is in $2\lambda\mathbb{Z}$. This constraint can be used after the support constraint in each step of the algorithm.

We observed that the rounding operation followed by PGD provides good recovery of $\mathbf{z}$ from the modulo samples for small $N_\lambda$, whereas, for large $N_\lambda$, the estimation tends to be more accurate at the edges of the support.

Using this observation, we propose a sequential approach to improve the accuracy of the estimation of the remaining samples. Starting from a given $N_\lambda$, let the PGD algorithm estimate of $\mathbf{z}$ be $\hat{\mathbf{z}}$. The estimate has support over $\mathcal{N}_\lambda$, and its values are integer multiples of $2\lambda$. In the absence of noise,

$$\mathbf{z}[n] = \hat{\mathbf{z}}[n], \quad n = \pm N_\lambda. \tag{15}$$

To estimate the remaining samples of $\mathbf{z}$ accurately, we define

$$\hat{\mathbf{f}} = \mathbf{f}_\lambda - \hat{\mathbf{z}}. \tag{16}$$

Combining (7) and (16),

$$\hat{\mathbf{f}} = \mathbf{f} + \mathbf{z} - \hat{\mathbf{z}}. \tag{17}$$

From (15) and (17) we have that $\hat{\mathbf{f}}[n] = \mathbf{f}[n]$, $|n| > N_\lambda - 1$. As a result, the new residual sequence $\mathbf{z} - \hat{\mathbf{z}}$ has support over $\{-(N_\lambda - 1), \cdots, (N_\lambda - 1)\}$, that is, $\mathbf{z} - \hat{\mathbf{z}} \in \mathcal{S}_{N_\lambda - 1}$ and $\mathbf{z} - \hat{\mathbf{z}} \in 2\lambda\mathbb{Z}$. Hence, $\hat{\mathbf{f}}$ has a similar decomposition as in (7) except for the fact that its values need not be in the range $[-\lambda, \lambda]$. Despite that, we can redefine the optimization problem as in (13) to estimate $\mathbf{z} - \hat{\mathbf{z}}$ from $\hat{\mathbf{f}}$ and use the PGD iterations in (14) to solve it. The residue $\mathbf{z} - \hat{\mathbf{z}}$ is correctly estimated for $n = \pm(N_\lambda - 1)$, from which $\mathbf{f}$ can be determined at those locations. The process is repeated until all the samples are estimated. The algorithm, refereed as $B^2R^2$, is summarized in

**Algorithm 1** $B^2R^2$ for recovery of BL signals from modulo samples.

**Input** $f_\lambda(nT_s)$ or $\mathbf{f}_\lambda$, $\lambda$, $\rho$ and $N_\lambda$
**Initialize:** $\hat{\mathbf{f}} = \mathbf{f}_\lambda$, $\mathbf{z}^0 \in S_{N_\lambda}$
**while** $N_\lambda > 0$ **do**
  **for** $k = 1$, $k$++, Until stopping criteria **do**
    $\mathbf{y}^k = \mathbf{z}^{k-1} - \gamma_k \mathcal{F}^*_\rho \mathcal{F}_\rho(\mathbf{z}^{k-1} - \hat{\mathbf{f}})$
    $\mathbf{z}^k = P_{S_{N_\lambda}}(\mathbf{y}^k)$
  **end for**
  $\hat{\mathbf{z}} = \mathbf{z}^k$, ▷ Estimation after applying PGD algorithm
  $\hat{\mathbf{z}} \leftarrow 2\lambda \left\lfloor \frac{[\hat{\mathbf{z}}/\lambda]}{2} \right\rceil$ ▷ rounding to $2\lambda\mathbb{Z}$
  $\hat{\mathbf{f}} \leftarrow \hat{\mathbf{f}} - \hat{\mathbf{z}}$
  $N_\lambda \leftarrow N_\lambda - 1$
  $\mathbf{z}^0 = P_{S_{N_\lambda}}(\hat{\mathbf{z}})$
**end while**
**Output:** $\mathbf{f} = \hat{\mathbf{f}}$

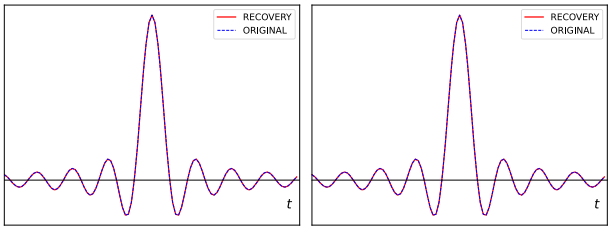


(a) $\lambda = 0.25, N_\lambda = 4$ (b) $\lambda = 0.20, N_\lambda = 9$

**Fig. 4.** Reconstruction of bandlimited signals from its modulo samples by using the $B^2R^2$ algorithm: Perfect reconstruction is achieved for both $N_\lambda = 4$ and $N_\lambda = 9$.

Algorithm 1. For initialization, we choose $\mathbf{z}^0$ as $P_{S_{N_\lambda}}\{\mathcal{F}^*_\rho \mathcal{F}_\rho \mathbf{f}_\lambda\}$ namely the inverse-partial DTFT of $\mathcal{F}_\rho \mathbf{z}$. To illustrate Algorithm 1, we consider the same example as shown in Fig. 3. We observe that, unlike the matrix inversion method, the $B^2R^2$ algorithm achieves perfect reconstruction for $\lambda = 0.25, 0.20$ as shown in Fig. 4.

The proposed algorithm (Algorithm 1) uses time-domain separation and frequency-domain separation properties to determine the residual signal. In contrast, the algorithm proposed in [17] uses these separation properties to directly predict the true samples from the folded ones. Specifically, the samples $f(nT_s)$, for all $|n| \le N_\lambda$ are predicted from $f(nT_s)$, for all $|n| > N_\lambda$. Hence, the algorithms are very different, although they use similar properties.

### 4.2. $B^2R^2$ algorithm for general operator

Next, we consider the general setting when non-linear samples are given by the operator $\mathcal{G}_\lambda$ as defined in (5). In this case, we define the residual signal as

$$z(nT_s) = g^{-1} \circ f_\lambda(nT_s) - f(nT_s) = u(nT_s) - f(nT_s), \tag{18}$$

where $u(nT_s) = g^{-1} \circ f_\lambda(nT_s)$. From the time and frequency separation, we obtain that

$$U(e^{\mathrm{j}\omega T_s}) = \sum_{n=-N_\lambda}^{N_\lambda} z(nT_s) e^{-\mathrm{j}nT_s\omega}, \tag{19}$$

for $\omega_m < |\omega| < \omega_s/2$. To estimate $z(nT_s)$ from $U(e^{\mathrm{j}\omega T_s})$, we consider an optimization framework as we did in the modulo case,

$$\min_{\mathbf{z}} \quad \mathrm{C}(\mathbf{z}) = \frac{1}{2}\|\mathcal{F}_\rho \mathbf{u} - \mathcal{F}_\rho \mathbf{z}\|^2 \quad \text{s.t.} \quad \mathbf{z} \in \mathcal{S}_{N_\lambda}. \tag{20}$$

Problem (20) can be solved using a PGD method as described in the modulo setting. Starting from an initial point $\mathbf{z}^0 \in \mathcal{S}_{N_\lambda}$, the steps at the $k$-th iteration are given by (14).

Although most of the steps of the $B^2R^2$ algorithm for a general operator remain the same as in Algorithm 1, the two steps differ. The first is the initialization $\hat{\mathbf{f}}$. For a general operator, we initialize to

$$\hat{\mathbf{f}} = g^{-1} \circ \mathbf{f}_\lambda. \tag{21}$$

The second difference is in imposing the structure of $\mathbf{z}$ to improve its accuracy. In Step-10 of Algorithm 1, we use the fact that elements of $\mathbf{z}$ should be an integer multiple of $2\lambda$. Similarly, for different operators $\mathcal{G}_\lambda$, the residual signal $\mathbf{z}$ could have additional structure.

For example, in clipping, if $f(nT_s) \ge \lambda$ then $f_\lambda(nT_s) = \lambda$. Hence, $z(nT_s) = f_\lambda(nT_s) - f(nT_s) \le 0$. Similarly, $z(nT_s) \ge 0$ when $f_\lambda(nT_s) = -\lambda$. Hence sign of $z(nT_s)$ can be determined from the clipped samples.

By using the structure in the sign of the $z(nT_s)$ we improve its estimation as

$$\begin{aligned}\hat{z}(nT_s) = &\min(0, \hat{z}(nT_s))\,\mathbf{1}_{[f_\lambda(nT_s)=\lambda]} \\ &+ \max(0, \hat{z}(nT_s))\,\mathbf{1}_{[f_\lambda(nT_s)=-\lambda]} \\ &+ 0\,\mathbf{1}_{[-\lambda<f_\lambda(nT_s)<\lambda]}.\end{aligned} \tag{22}$$

For clipping, the three conditions $f_\lambda(nT_s) = \lambda$, $f_\lambda(nT_s) = -\lambda$, and $\lambda < f_\lambda(nT_s) < \lambda$ are mutually exclusive and one of them is always true for any folded sample. In (22), we set the values of $z(nT_s)$ to zero when the sign conditions are not satisfied. Therefore, for clipping, we replace the operation in Step-10 of $B^2R^2$ algorithm with the approximation in (22).

To summarize, in the $B^2R^2$ algorithm for general operators, we use the initialization in (21) together with a suitable approximation in Step-10. This generalized algorithm is designed for a general operator where clipping, companding, and modulo are special cases. Thus, it can recover bandlimited signals from samples of all these operators. Importantly, the change in an ADC (together with the operator) does not require a change in the algorithm.

The proposed method requires knowledge of $N_\lambda$. In Appendix B, we discuss several approaches to compute $N_\lambda$ for bandlimited signals.

### 4.3. Complexity analysis

To determine the algorithm's computational complexity, let $L$ denote the number of samples of the bandlimited signal. Further, let $\mathcal{H}_\rho$ denote a high-pass operation equivalent to the operator $\mathcal{F}_\rho^*\mathcal{F}_\rho$. With these notations, the $k$-th iteration of the PGD step is given as

$$\mathbf{z}^k = P_{\mathcal{S}_{N_\lambda}}(\mathbf{z}^{k-1}) - P_{\mathcal{S}_{N_\lambda}}(\mathcal{H}_\rho(\mathbf{z}^{k-1} - \hat{\mathbf{f}})).$$

The vectors $\mathbf{z}^{k-1}$ and $\mathcal{H}_\rho(\mathbf{z}^{k-1} - \hat{\mathbf{f}})$ are of length $L$, whereas, their projected versions are of length $2N_\lambda + 1$. Hence, the above operation involves $L + 2N_\lambda + 1$ additions, which includes $L$ additions between $\mathbf{z}^{k-1}$ and $\hat{\mathbf{f}}$, and $2N_\lambda + 1$ between the two projections. Next, we consider the complexity of the operator $\mathcal{H}_\rho$. The operation is realized by using a highpass filter of length $M$ and convolving it with the vector $\mathbf{z}^{k-1} - \hat{\mathbf{f}}$. Convolution results in a vector of length $M + L - 1$. Then, we consider the middle part of the filtered sequence, which will have length $L$. The convolution is computed in $O(LM)$ operations. As a result, for $T$ inner iterations of the PGD algorithm, the total operations scale as $O(T(LM + N_\lambda))$. Given that our algorithm's primary loop traverses $N_\lambda, N_\lambda - 1, \ldots, 1$, the overall complexity can be represented as $O(T(LM + N_\lambda^2))$.

## 5. Simulation results

In this section, we present numerical results of different methods for recovering a bandlimited signal from the nonlinear samples. We first consider recovery in the absence of noise by using the proposed $B^2R^2$ algorithm. We then treat the noisy setting, comparing the proposed and existing approaches for reconstructing signals from modulo samples. We demonstrate the robustness to noise of the $B^2R^2$ algorithm for different parameters of $\lambda$ and the over-sampling factor.

### 5.1. Signal reconstruction from non-linear samples in the absence of noise

In this experiment, our goal is to demonstrate that the $B^2R^2$ algorithm perfectly reconstructs bandlimited signals from different nonlinear samples. Specifically, we consider the non-linearities discussed in Fig. 1, namely, clipping (cf. (4)), modulo operation as in (3), and a $\mu$-law modulo operator. Let $\lambda = 0.25$ for all these operators. Figs. 5(a), (b), and (c) depict a bandlimited signal (in blue) and outputs of non-linear operators (in red). The true signals with corresponding recovered signals are shown in Figs. 5(d), (e), and (f). For reconstruction from clipped samples, we used an OF = 10, and the rest of the two operators OF = 2 was used. This shows that it is difficult to reconstruct from the clipped samples compared to modulo samples. Overall, we observe that the $B^2R^2$ algorithm recovers the original signal perfectly from the samples of different non-linear operators.

### 5.2. Presence of noise

Next, we assess the performance of the $B^2R^2$ algorithm as a function of OF, $\lambda$, and noise level. Here, we focus on only the modulo operator as it enables us to compare the $B^2R^2$ method with the recently published algorithms [15,17]. Specifically, we compare $B^2R^2$ algorithm with the *higher-order differences* (HOD) approach [15] and *Chebyshev polynomial filter*-based (CPF) method [17]. We examine the reconstruction problem from the following noisy measurements

$$\tilde{f}_\lambda(nT_s) = f_\lambda(nT_s) + v(nT_s) = \mathcal{M}_\lambda f(nT_s) + v(nT_s), \tag{23}$$

where $v(nT_s)$ denotes noise. In the experiments, we normalize the bandlimited signals to have a maximum amplitude of one. In the simulations SNR is computed as $\text{SNR} = 20\log\left(\frac{||f_\lambda(nT_s)||}{||v(nT_s)||}\right)$. The reconstruction accuracy of different algorithms is compared in terms

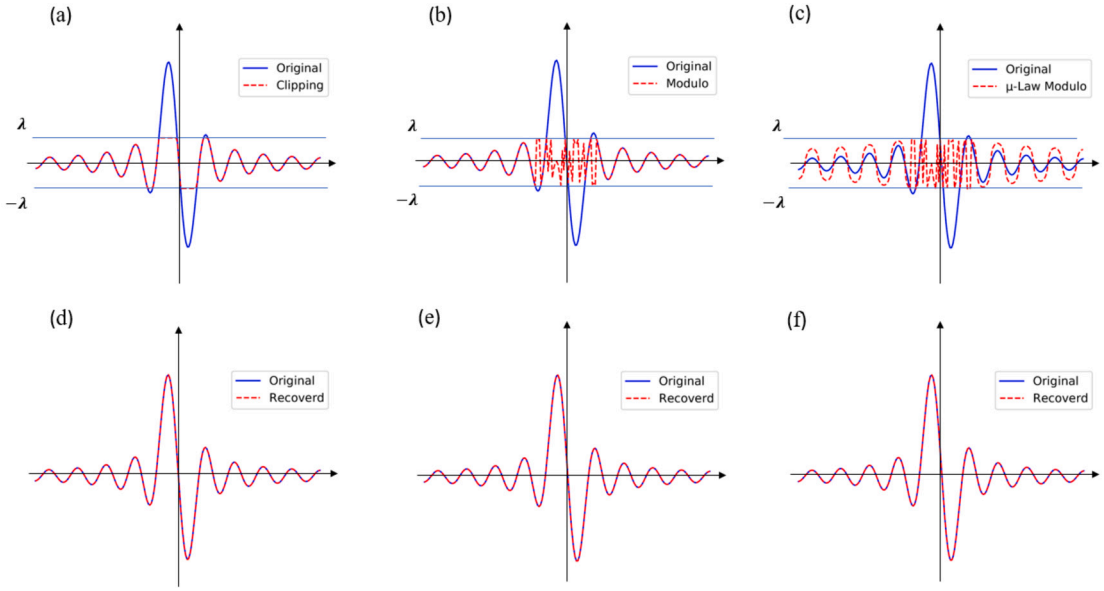


**Fig. 5.** Reconstruction of bandlimited signals from non-linear samples using $B^2R^2$ algorithm; Top row shows original signals and outputs of (a) clipping, (b) modulo operation, and (c) $\mu$-Law modulo; Bottom row shows recovery using $B^2R^2$ from samples of (d) clipping, (e) modulo operator, and (f) $\mu$-Law modulo recovery.

of normalized mean-squared error (MSE) as $\frac{\sum|f(nT_s)-\hat{f}(nTs)|^2}{\sum|f(nT_s)|^2}$, where $\hat{f}(nT_s)$ denotes the estimate of $f(nT_s)$. For each noise level, 1000 independent noise realizations were generated, and the average MSE was computed for them. In all experiments, we consider a synthetic bandlimited signal of length 1024. The samples are generated as a linear combination of sinc functions:

$$f(nT_s) = \sum_{k=-10}^{9} c_k \,\mathrm{sinc}(\omega_m T_s(n-5k)). \quad n = [-512, 511],$$

where $\omega_m = 1$ rad/sec. The coefficients $\{c_k\}$ were drawn independently from a uniform distribution on $[-1, 1]$ for each noise realization. The signals are normalized to have a maximum value of one. In the simulations, the order of the Chebyshev polynomial filter is chosen according to formula (9) in [17]. For the HOD method, the order of the difference operator is computed using formula (14) in [15]. The structure of the generated signals is a sum of sinc functions with random coefficients. We examine both bounded and unbounded noises.

### 5.2.1. *Bounded noise*

For bounded noise, we assume that the noise is uniformly distributed with zero mean and $|v(nT_s)| \leq \sigma$. We compare the algorithms for different SNRs and OFs with fixed $\lambda$. Fig. 6, 7, and 8 show MSEs of the algorithms for $\lambda = 0.2, 0.1$, and $0.05$, respectively.

We observe that the HOD method is unable to reconstruct the signals (with MSE on the order of 60 dB) for noise levels and $\lambda$s considered in the simulations. This is because a sufficient condition for the HOD algorithm to recover the signal in the absence of noise is that OF $\geq 17$. In the presence of noise, a larger amount of oversampling is required, and hence, in this simulation setting, where OF $\leq 10$, the method fails. Both $B^2R^2$ and CPF algorithms reconstruct the signal with lower MSEs. To ascertain the claim, we perform simulations for OF $\geq 10$ with $\lambda = 0.1$ and $\lambda/\sigma = 10$. The MSEs for the three algorithms are shown in Fig. 9. We observe that for OF $\geq 25$, the HOD method can reconstruct the signal in this particular setting, whereas, as expected, both $B^2R^2$ and CPF methods reconstruct the signal for lower OFs.

Comparing the $B^2R^2$ and CPF methods, we observe that $B^2R^2$ results in lower MSE. For a better visualization, a comparison of MSEs of these two algorithms for OF $= 4$ and 8 in Fig. 10. For OF $= 4$, the $B^2R^2$ algorithm has $10 - 40$ dB lower MSE than the CPF approach for different noise levels.

### 5.2.2. *Unbounded noise*

In these experiments, we assume that the noise samples $v(nT_s)$ are independent and identically distributed Gaussian random variables with zero mean. The variance is set to achieve the desired SNR. We compare the algorithms for different SNRs and OFs with fixed $\lambda$. Fig. 11, 12 and 13 show MSE of the algorithms for $\lambda = 0.2, 0.1, 0.05$, respectively. As in the case of bounded noise, the HOD method cannot recover the signal for this experimental setup. Comparing the rest of the methods, the $B^2R^2$ algorithm results in lower MSE than that of the CPF method for a given $\lambda$, MSE, and OF.

For a better visualization, we compared the $B^2R^2$ and CPF methods in terms of MSE for OF $= 4$ and OF $= 8$ in Fig. 14. For OF $= 4$, we note that for low SNR values, the $B^2R^2$ algorithm results in $10 - 30$ dB lower MSE when compared to the CPF approach.

Next, we compare the three methods with a recently published algorithm that uses signal averages rather than the instantaneous samples for digital representation (See Algorithm 2 in [34]). We refer to this algorithm as Local Average where the continuous modulo

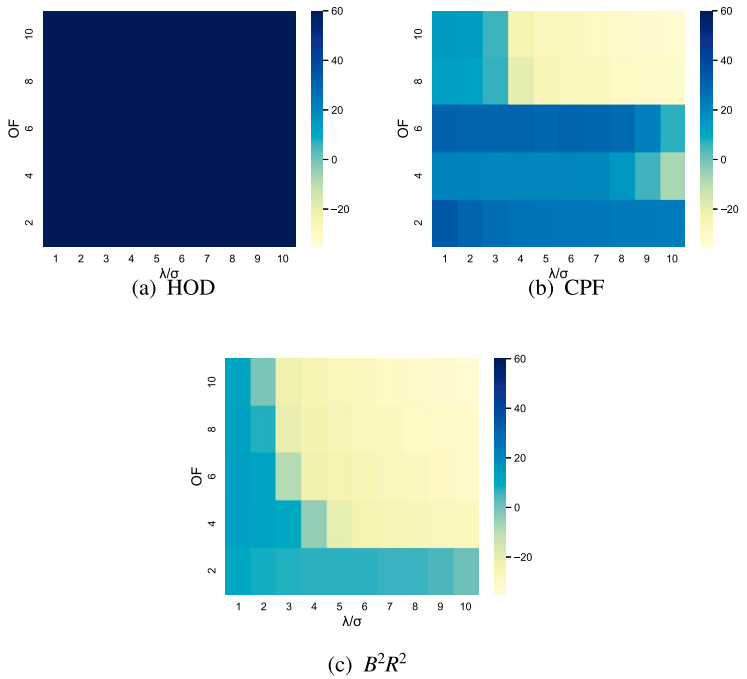


**Fig. 6.** Comparison of algorithms (with bounded noise) in terms of MSE when recovering a bandlimited signal from modulo samples with $\lambda = 0.2$. For a given SNR and OF, $B^2R^2$ has the lowest MSE.

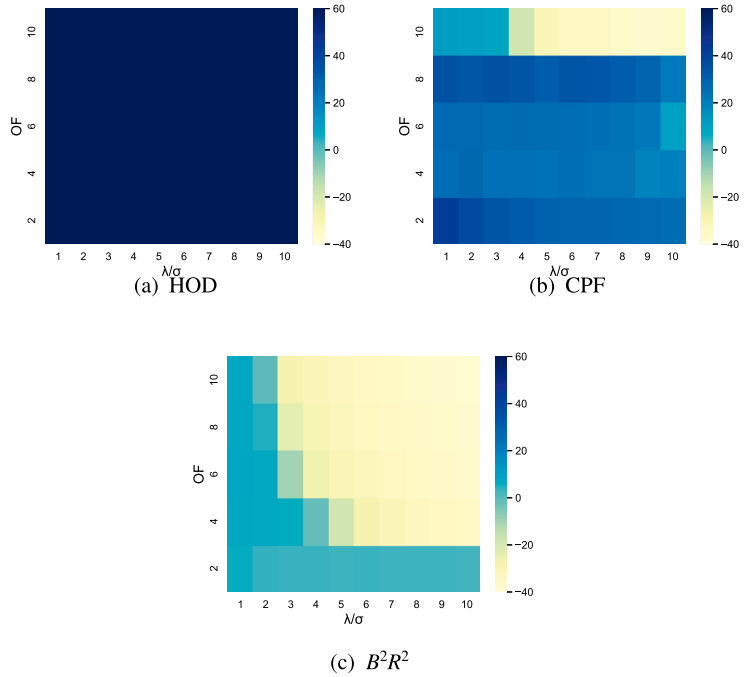


**Fig. 7.** Comparison of algorithms (with bounded noise) in terms of MSE when recovering a bandlimited signal from modulo samples with $\lambda = 0.1$. For a given SNR and OF, $B^2R^2$ has the lowest MSE.

signal is sampled with an averaging filter $\psi(t) = \frac{1}{2v}\mathbf{1}_{[-v,v]}(t)$ where $v = 0.01$. The modulo parameter is $\lambda = 0.125$. Figs. 15 and 16 show MSEs for different algorithms as a function of oversampling factor (OF) for SNR = 15 dB and 30 dB, respectively. We observe that the local-average approach for SNR = 30 dB results in a large error for OF $< 20$. The local average method fails to recover the signal for SNR = 15 dB.

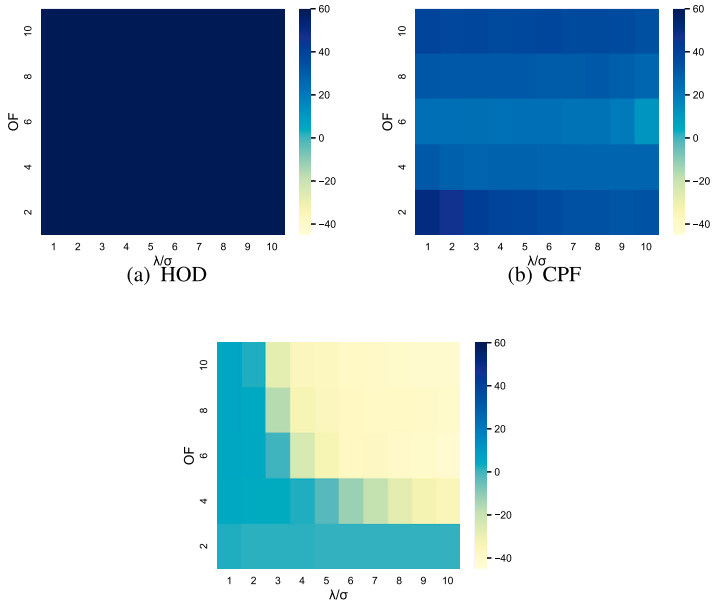


(a) HOD (b) CPF

(c) $B^2R^2$

**Fig. 8.** Comparison of algorithms (with bounded noise) in terms of MSE when recovering a bandlimited signal from modulo samples with $\lambda = 0.05$. For a given SNR and OF, $B^2R^2$ has the lowest MSE.

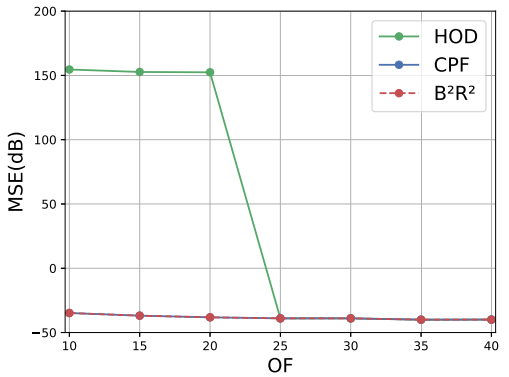


**Fig. 9.** Comparison of algorithms in terms of MSE in recovering a bandlimited signal from uniform noisy modulo samples with $\lambda = 0.1$, and $\lambda/\sigma = 10$; The higher-order difference approach has an error of $-40$ dB for OF $\geq 25$ whereas the remaining methods achieve $-40$ dB error for OF $= 10$.

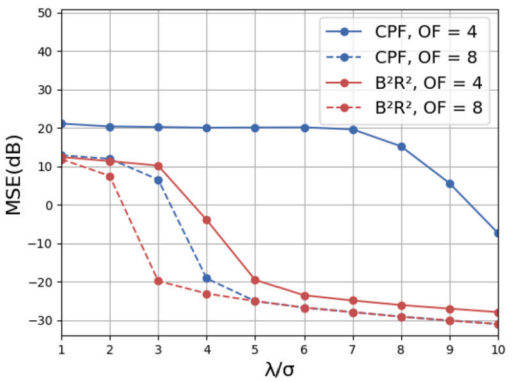


**Fig. 10.** Comparison of CPF and $B^2R^2$ algorithms (with bounded noise) in terms of MSE when recovering a bandlimited signal from modulo samples with $\lambda = 0.2$ and OF $= 4, 8$. For a given ratio $\lambda/\sigma$, $B^2R^2$ has the lowest MSE.

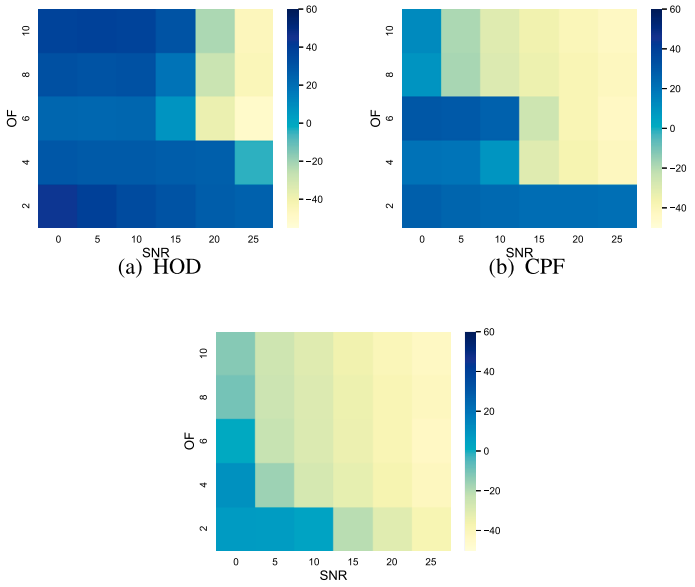


(a) HOD (b) CPF

(c) $B^2R^2$

**Fig. 11.** Comparison of algorithms (with unbounded noise) in terms of MSE when recovering a bandlimited signal from modulo samples with $\lambda = 0.2$. For a given SNR and OF, $B^2R^2$ has the lowest MSE.

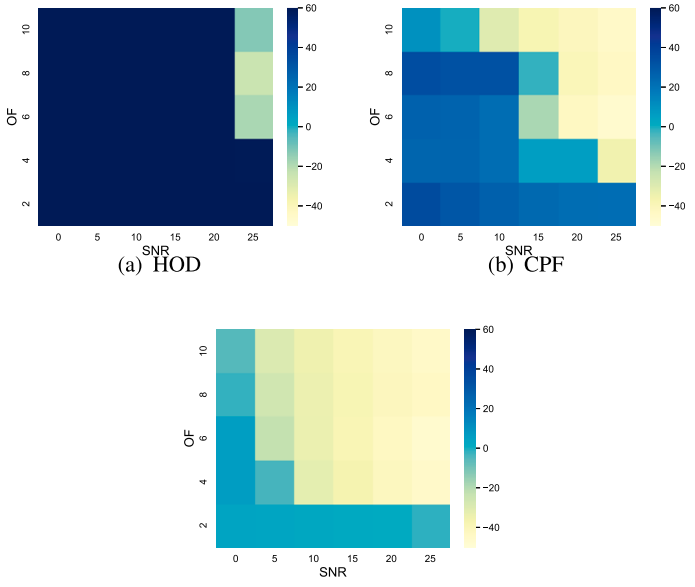


(a) HOD (b) CPF

(c) $B^2R^2$

**Fig. 12.** Comparison of algorithms (with unbounded noise) in terms of MSE when recovering a bandlimited signal from modulo samples with $\lambda = 0.1$. For a given SNR and OF, $B^2R^2$ has the lowest MSE.

### 5.3. Unbounded noise before modulo

Here, our consideration involved adding noise before applying the modulo operation. In this scenario, the signal samples undergoing modulo folding are expressed as follows:

$$\tilde{f}(nT_s) = f(nT_s) + v(nT_s), \tag{24}$$

where $\{v(nT_s)\}_{n\in\mathbb{Z}}$ represents independent and identically distributed Gaussian samples with zero mean and a standard deviation of $\sigma$. Subsequently, the inputs modulo samples are obtained as $\tilde{f}_\lambda(nT_s) = \mathcal{M}_\lambda \tilde{f}(nT_s)$. We estimated $f(nT_s)$ using the $B^2R^2$, CPF, and

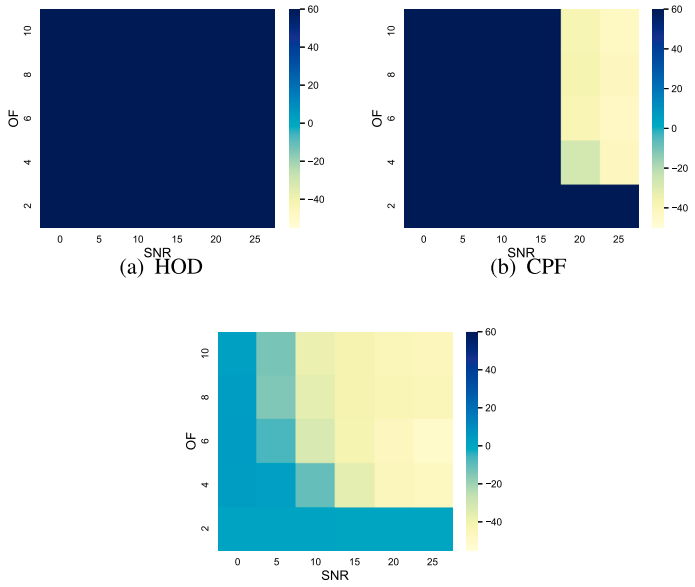


**Fig. 13.** Comparison of algorithms (with unbounded noise) in terms of MSE when recovering a bandlimited signal from modulo samples with $\lambda = 0.05$. For a given SNR and OF, $B^2R^2$ has the lowest MSE.

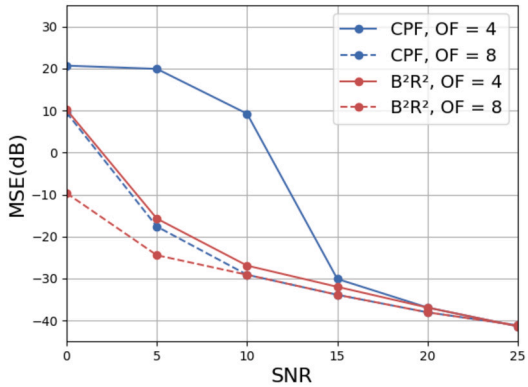


**Fig. 14.** Comparison of CPF and $B^2R^2$ algorithms (with unbounded noise) in terms of MSE while recovering signal from modulo samples with $\lambda = 0.2$ and OF $= 4, 8$. For a given SNR, $B^2R^2$ has lowest MSE.

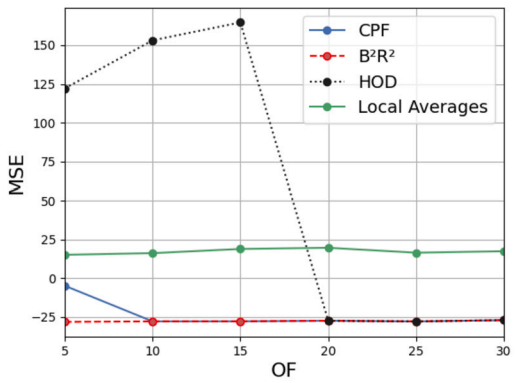


**Fig. 15.** Comparison of algorithms, including local average method, (with unbounded noise) in terms of MSE when recovering a bandlimited signal from modulo samples with $\lambda = 0.125$ and SNR $= 15$ dB.

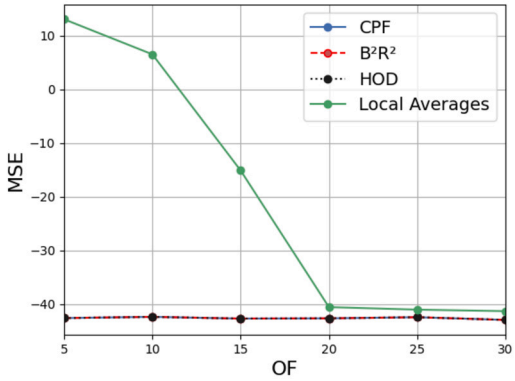


**Fig. 16.** Comparison of algorithms, including local average method, (with unbounded noise) in terms of MSE when recovering a bandlimited signal from modulo samples with $\lambda = 0.125$ and SNR = 30 dB.

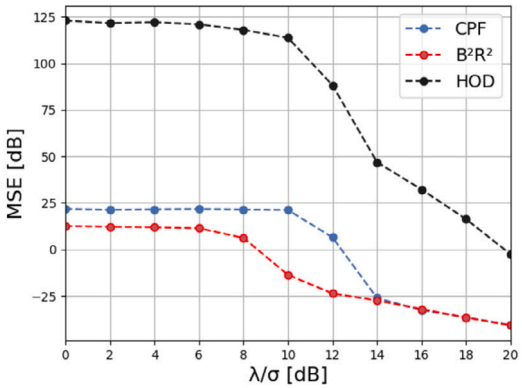


(a) OF = 4

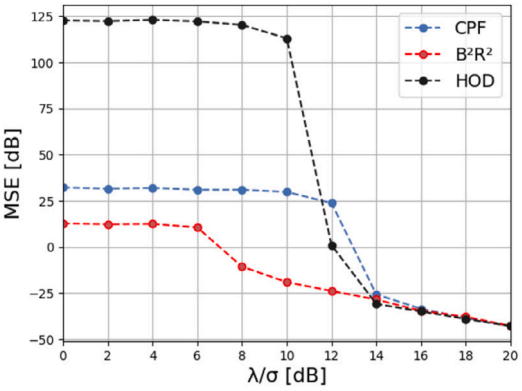


(b) OF = 6

**Fig. 17.** Comparison of algorithms (with unbounded noise added before the modulo operation) in terms of MSE when recovering a bandlimited signal from modulo samples with $\lambda = 0.2$. For a given SNR and OF, $B^2R^2$ has the lowest MSE.

HOD methods on $\tilde{f}_\lambda$. The normalized MSEs are depicted in Fig. 17 for various methods while ensuring $|f(t)| \leq 1$ and maintaining $\lambda = 0.2$. The signal was then sampled for OF $= 4, 6$.

We noticed that the $B^2R^2$ method exhibits the lowest error among the three approaches. However, compared to when the noise was introduced after the modulo operation (refer to Fig. 14 of the manuscript), the MSE in this scenario is higher for any given Oversampling Factor (OF) and noise level across all methods. This discrepancy arises because even a slight addition of noise to the input signal can significantly alter the residual signal $z(t)$, leading to a notable error.

To tackle this challenge, denoising techniques were introduced in [41–43], where the authors consider adding noise before sampling as shown in (24) for smooth signals. Recognizing that consecutive sequence samples $\tilde{f}_\lambda(nT_s)$ might be widely dispersed in value but closer in the angular domain, the authors proposed a denoising algorithm employing a quadratically constrained quadratic

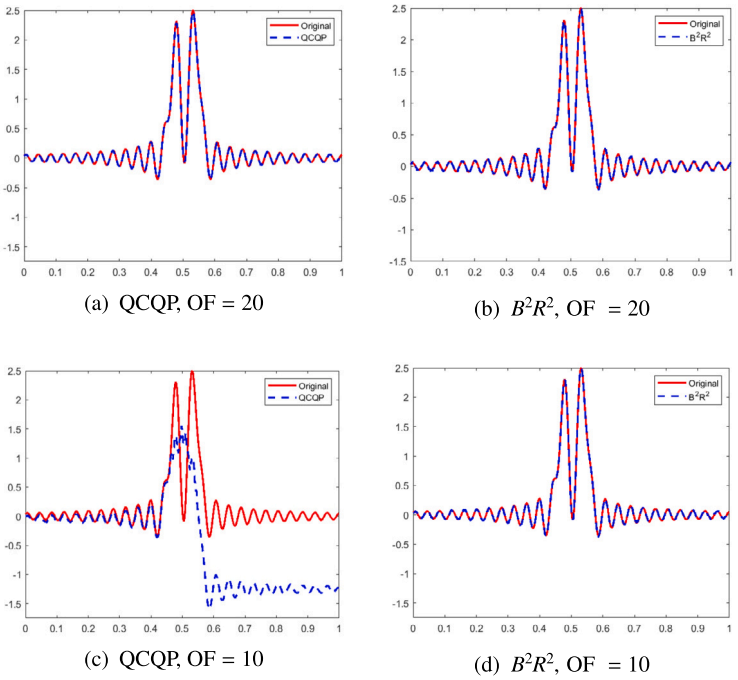


(a) QCQP, OF = 20 (b) $B^2R^2$, OF = 20

(c) QCQP, OF = 10 (d) $B^2R^2$, OF = 10

**Fig. 18.** A comparison of QCQP-based algorithm [42] with the $B^2R^2$ algorithm.

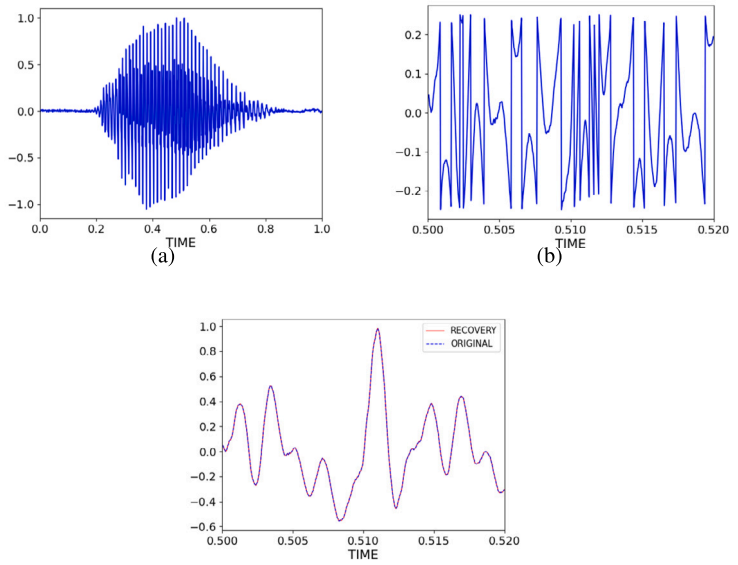


**Fig. 19.** Reconstruction of speech signals by using the $B^2R^2$ algorithm: (a) speech signal; (b) zoom-in of folded speech; (c) true and recovered signal by using $B^2R^2$ algorithm.

program (QCQP). The objective is to estimate $f_\lambda(nT_s)$ from $\tilde{f}_\lambda(nT_s)$. The simulation results in [41–43] primarily focused on denoising smooth signals.

In the following, we have compared our method to the QCQP-based approach as proposed in [42]. To align with the setting as in [42], we use $\lambda = \frac{1}{2}$ and set $\|f\|_\infty = 2.5$. In Fig. 18, we illustrate the recovery of a bandlimited signal that sampled with an OF = 20 and 10. As we can observe, both QCQP and $B^2R^2$ methods recover the signal faithfully for OF = 20, but the QCQP fails for OF = 10. In both examples, the SNR was 35 dB.

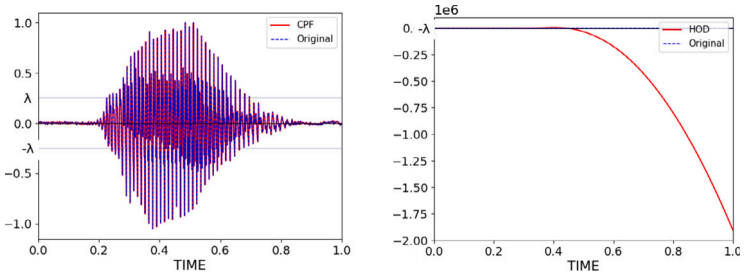


(a) CPF (b) HOD

**Fig. 20.** Reconstruction of the speech signal from its modulo samples using CPF and HOD algorithms. While the CPF algorithm is able to reconstruct the speech signal faithfully, the HoD method fails due to insufficient oversampling.

### *5.4. Real signals*

In this subsection, we present a recovery example of a real speech signal. Specifically, we consider a speech signal followed by a low-pass filter with a cutoff frequency of 1 kHz and normalization to get a maximum value of one, as shown in Fig. 19(a). The signal is folded with $\lambda = 0.25$ and sampled at 4 kHz. In Fig. 19(b) and Fig. 19(c), we show the modulo and the estimated signal by applying the $B^2R^2$ algorithm. For a better analysis, we present the results for the interval $[0.5, 0.52]$. We observe perfect recovery (up to machine precision).

In Fig. 20, we plot the modulo signal on top of the original one for the CPF and HoD approaches. As observed, the $B^2R^2$ and CPF methods achieved a perfect recovery (up to machine precision), whereas the HOD algorithm failed to recover the speech signal.

## 6. Acknowledgments

This research was partially supported by the Israeli Council for Higher Education (CHE) via the Weizmann Data Science Research Center, by a research grant from the Estate of Tully and Michele Plesser, by the European Union's Horizon 2020 research and innovation program under grant No. 646804-ERC-COG-BNYQ, by The Israel Science Foundation under grant no. 0100101, and by the QuantERA grant C'MON-QSENS.

## 7. Conclusion

We propose a nonlinear operator that can be used to address the dynamic range issue of ADCs. Our approach generalizes existing operators such as companding and modulo. We show that bandlimited signals can be perfectly reconstructed from the samples of the proposed nonlinear operator, provided that the sampling rate is greater than the Nyquist rate. We also suggest a robust algorithm, referred to as $B^2R^2$, to recover the true samples from the nonlinear samples. Our results show that the $B^2R^2$ algorithm operates at a lower sampling rate compared to existing approaches for different noise levels and dynamic ranges and results in lower recovery error.

## Appendix A. Proof of Theorem 1

In this appendix, we prove Theorem 1. We first present the proof for the necessary part and then discuss sufficiency.

*Necessary part* Let $\omega_s = \frac{2\pi}{T_s}$ denote the sampling rate in rad/sec. To prove the necessary condition on the sampling rate, we consider two cases: (i) Sampling below the Nyquist rate: $\omega_s = \frac{2\pi}{T_s} < 2\omega_m$ and (ii) Sampling at the Nyquist rate: $\omega_s = 2\omega_m$. When the bandlimited signal $f(t)$ is sampled below the Nyquist rate then there exists another signal $\hat{f}(t) \in L^2(\mathbb{R}) \cap B_{\omega_m}$ such that $f(nT_s) = \hat{f}(nT_s)$, for all $n \in \mathbb{Z}$ due to aliasing. This implies that the samples of the framework shown in Fig. 2 are the same for inputs $f(t)$ and $\hat{f}(t)$, that is, $f_\lambda(nT_s) = \hat{f}_\lambda(nT_s)$, for all $n \in \mathbb{Z}$. Hence the signal $f(t)$ is not uniquely identifiable from $f_\lambda(nT_s)$ for $\omega_s < 2\omega_m$.

Next, consider sampling at the Nyquist rate $\omega_s = 2\omega_m$. We show that a signal $f(t)$ exists, which is not uniquely identifiable. In other words, given $f(t)$ there exists another bandlimited signal $\hat{f}(t) \in L^2(\mathbb{R}) \cap B_{\omega_m}$ such that $f_\lambda(nT_s) = \hat{f}_\lambda(nT_s)$, for all $n \in \mathbb{Z}$. Consider an $f(t) \in L^2(\mathbb{R}) \cap B_{\omega_m}$ such that $|f(n_0T_s)| > \lambda$ for some $n_0 \in \mathbb{Z}$. For example, for $f(t) = 2\lambda \operatorname{sinc}\left(\frac{t-n_0T_s}{T_s}\right)$ satisfies the mentioned sampling conditions.

We construct $\hat{f}(t)$, from the samples $f(nT_s)$, by defining its Nyquist rate samples as

$$\hat{f}(nT_s) = \begin{cases} g^{-1} \circ \mathcal{G}_\lambda f(nT_s), & n = n_0, \\ f(nT_s), & \text{otherwise}, \end{cases} \tag{A.1}$$

where $g^{-1}(\cdot)$ is the inverse of $g(\cdot)$ (cf. (5)). The range and domain of the functions $g(\cdot)$, $g^{-1}(\cdot)$ are given by the interval $[-\lambda, \lambda]$.

Since $|\mathcal{G}_\lambda f(n_0T_s)| \leq \lambda$ (cf. (6)), then from the aforementioned range of $g^{-1}(\cdot)$, we infer that

$$|\hat{f}(n_0T_s)| \leq \lambda. \tag{A.2}$$

Hence $f(n_0T_s) \neq \hat{f}(n_0T_s)$ and thus $f(t) \neq \hat{f}(t)$.

The signal $\hat{f}(t)$ is in $B_{\omega_m}$ by construction. Next, we show that it is also in $L^2(\mathbb{R})$. From Parseval's formula, we have that

$$\int_{-\infty}^{\infty} |\hat{f}(t)|^2 \mathrm{d}t = T_s \sum_{n\in\mathbb{Z}} |\hat{f}(nT_s)|^2, \tag{A.3}$$

$$= T_s \sum_{n\in\mathbb{Z}} |f(nT_s)|^2 + T_s|\hat{f}(n_0T_s)|^2 - T_s|f(n_0T_s)|^2. \tag{A.4}$$

Since $f(t) \in L^2(\mathbb{R})$ the first and the third terms on the right-hand side are finite, and from (A.2) we have that $\hat{f}(t) \in \mathbb{L}^2(\mathbb{R})$.

Next, consider the nonlinear samples of $\hat{f}(t)$. Since $f(nT_s) = \hat{f}(nT_s), n \in \mathbb{Z}\backslash\{n_0\}$, we have that $\hat{f}_\lambda(nT_s) = f_\lambda(nT_s)$ for all $n \in \mathbb{Z}\backslash\{n_0\}$. For $n = n_0$, we have the following equalities.

$$\begin{aligned}
\hat{f}_\lambda(n_0T_s) &= \mathcal{G}_\lambda \hat{f}(n_0T_s), \\
&= g \circ \hat{f}(n_0T_s), \quad \text{(from (5) and (A.2))} \\
&= g \circ g^{-1} \circ \mathcal{G}_\lambda f(n_0T_s), \quad \text{(from (A.1) )} \\
&= \mathcal{G}_\lambda f(n_0T_s) = f_\lambda(n_0T_s).
\end{aligned} \tag{A.5}$$

This shows that there exist two different bandlimited functions $f(t)$ and $\hat{f}(t)$ whose non-linear samples are identical when measured at the Nyquist rate. This proves that it is necessary to sample above the Nyquist rate.

*Sufficient part* We prove this part by contradiction. Assume that there exist two different bandlimited signals $f_1(t), f_2(t) \in L^2(\mathbb{R}) \cap B_{\omega_m}$ with the same non-linear samples, sampled above the Nyquist rate. That is,

$$\mathcal{G}_\lambda f_1(nT_s) = \mathcal{G}_\lambda f_2(nT_s), \forall n \in \mathbb{Z}. \tag{A.6}$$

Since $f_1(t)$ and $f_2(t)$ are bandlimited and have finite energy, their continuous Fourier transforms $F_1(\omega)$ and $F_2(\omega)$ have finite energy (From Parseval's theorem) and have finite support. Therefore, both $F_1(\omega)$ and $F_2(\omega)$ are absolutely integral (by applying Hölder's inequality). Hence, from the Riemann–Lebesgue lemma, we have that $|f_k(t)| \to 0$ as $|t| \to \infty$ for $k = 1, 2$. In other words, for a given $\lambda$ there exist an integer $N_\lambda$ such that

$$|f_k(nT_s)| < \lambda, \quad \forall |n| > N_\lambda, \quad k = 1, 2. \tag{A.7}$$

From (5) and (A.6), for $|n| > N_\lambda$ we have that

$$g \circ f_1(nT_s) = g \circ f_1(nT_s), \tag{A.8}$$

$$\implies f_1(nT_s) = f_2(nT_s), \tag{A.9}$$

where the last equality is because $g$ is invertible.

Next, consider an $\omega_m$-bandlimited function $h(t) = f_1(t) - f_2(t)$. Since $h(nT_s) = f_1(nT_s) - f_2(nT_s)$, from (A.9) we have that

$$h(nT_s) = 0, \quad |n| > N_\lambda. \tag{A.10}$$

The DTFT of $h(nT_s)$ is given as

$$H(e^{j\omega T_s}) = \sum_{n=-\infty}^{\infty} h(nT_s) e^{-\mathrm{j}nT_s\omega} \tag{A.11}$$

$$= \sum_{n=-N_\lambda}^{N_\lambda} h(nT_s) e^{-\mathrm{j}nT_s\omega} \tag{A.12}$$

$$= \frac{1}{T_s} \sum_{k=-\infty}^{\infty} H\left(\omega - k\omega_s\right), \tag{A.13}$$

where $H(\omega)$ is the CTFT of $h(t)$. Since $H(\omega) = 0, \omega \notin [-\omega_m, \omega_m]$ and $\omega_s > 2\omega_m$, we note that

$$H(e^{\mathrm{j}\omega}) = \sum_{n=-N_\lambda}^{N_\lambda} h(nT_s) e^{-\mathrm{j}nT_s\omega} = 0, \text{ for } \omega \in [\omega_m, \omega_s/2]. \tag{A.14}$$

Since $H(e^{j\omega})$ is a trigonometric polynomial and it is equal to zero over an interval, then by using the identity theorem [44, Page 122] we have that $H(e^{j\omega}) = 0$ for all $\omega \in \mathbb{R}$. This implies that $h(nT_s) = 0$, for all $n \in \mathbb{Z}$. Hence, $f_1(nT_s) = f_2(nT_s)$, for all $n \in \mathbb{Z}$ and therefore $f_1(t) = f_2(t)$, which contradicts our initial assumption. A similar line of proof is used in [45] to derive sufficient conditions for bandlimited signals from their modulo samples.

## Appendix B. Computation of $N_\lambda$

The Riemann-Lebesgue lemma implies that finite energy bandlimited signals decay with time. This principle was also used in [17]. Here we discuss several methods to determine $N_\lambda$ for finite energy bandlimited signals.

The first approach is to consider the class of bandlimited signals $C_{\omega_m,E,T_0,r}$ which is a subset of $L^2(\mathbb{R}) \cap B_{\omega_m}$ as in [17]. Any function $f(t) \in C_{\omega_m,E,T_0,r}$ is bandlimited to frequency interval $[-\omega_m, \omega_m]$ and has maximum energy $E$. In addition, the signal has the following decay properties:

$$|f(t)| < |t|^{-r}, \quad \forall |t| > T_0. \tag{B.1}$$

If we consider signals in the restricted space $C_{\omega_m,E,T_0,r}$ for modulo sampling then $N_\lambda$ is given as [17]

$$N_\lambda = T_s^{-1} \max\{T_0, \lambda^{-1/r}\},$$

where $T_s$ is the sampling interval.

Next, we propose an alternative approach that does not require the exact decay constant $r$ for bandlimited signals but assumes that maximum energy $E$ is known. Ideally, there are infinite samples of bandlimited signals. However, in practice, we consider a finite number of samples by ignoring samples that are below a certain threshold, such as machine precision. Specifically, we consider samples $f(nT_s)$ for $n \in [-N_\epsilon, \cdots, N_\epsilon]$ where $\epsilon$ is machine precision and $N_\epsilon$ is known.

In the $B^2R^2$ algorithm, one can choose $N_\lambda$ to be $N_\epsilon$. However, since $\epsilon \ll \lambda$ we have that $N_\epsilon \gg N_\lambda$. In this case, $B^2R^2$ becomes computationally expensive due to incorrect estimation of $N_\lambda$. The estimation can be improved by considering the following inequality from [46]

$$|f(t+\tau) - f(t)| \leq \omega_m \tau \sqrt{\frac{E\omega_m}{3\pi}}, \quad \forall \tau \in \mathbb{R}. \tag{B.2}$$

By using the inequalities $|f(N_\epsilon T_s)| \leq \epsilon$ and $|f(N_\lambda T_s)| \geq \lambda$ in (B.2) we have

$$\omega_m \sqrt{\frac{E\omega_m}{3\pi}} (N_\epsilon - N_\lambda) T_s \geq |f(N_\epsilon T_s) - f(N_\lambda T_s)| \geq \lambda - \epsilon. \tag{B.3}$$

From the above inequality, a lower bound on $N_\lambda$ is given as

$$N_\lambda \leq N_\epsilon - \frac{1}{T_s \omega_m} \sqrt{\frac{3\pi}{E\omega_m}} (\lambda - \epsilon). \tag{B.4}$$

Unlike the first approach, this method does not require the knowledge of decay constant $r$.

## Data availability

Data will be made available on request.

## References


[1] R. Marks, Restoring lost samples from an oversampled band-limited signal, IEEE Trans. Acoust. Speech Signal Process. 31 (3) (1983) 752–755, https://doi.org/10.1109/TASSP.1983.1164101.

[2] R. Marks, D. Radbel, Error of linear estimation of lost samples in an oversampled band-limited signal, IEEE Trans. Acoust. Speech Signal Process. 32 (3) (1984) 648–654, https://doi.org/10.1109/TASSP.1984.1164370.

[3] J. Armstrong, Peak-to-average power reduction for OFDM by repeated clipping and frequency domain filtering, Electron. Lett. 38 (1) (2002) 246–247.

[4] S.H. Han, J.H. Lee, An overview of peak-to-average power ratio reduction techniques for multicarrier transmission, IEEE Wirel. Commun. 12 (2) (2005) 56–65.

[5] J.S. Abel, J.O. Smith, Restoring a clipped signal, in: Proc. IEEE Intl. Conf. Acoust., Speech and Signal Process. (ICASSP), vol. 3, 1991, pp. 1745–1748.

[6] R. Rietman, J.-P. Linnartz, E.P. de Vries, Clip correction in wireless LAN receivers, in: Proc. European Conf. Wireless Tech., 2008, pp. 174–177.

[7] J.P.A. Pérez, S.C. Pueyo, B.C. López, Automatic Gain Control, Springer, 2011.

[8] D. Mercy, A review of automatic gain control theory, Radio Electron. Eng. 51 (11–12) (1981) 579–590.

[9] H.J. Landau, On the recovery of a band-limited signal, after instantaneous companding and subsequent band limiting, Bell Syst. Tech. J. 39 (2) (1960) 351–364, https://doi.org/10.1002/j.1538-7305.1960.tb01604.x.

[10] H.J. Landau, W.L. Miranker, The recovery of distorted band-limited signals, J. Math. Anal. Appl. 2 (1) (1961) 97–104.

[11] D. Park, J. Rhee, Y. Joo, A wide dynamic-range CMOS image sensor using self-reset technique, IEEE Electron Device Lett. 28 (10) (2007) 890–892, https://doi.org/10.1109/LED.2007.905396.

[12] K. Sasagawa, T. Yamaguchi, M. Haruta, Y. Sunaga, H. Takehara, H. Takehara, T. Noda, T. Tokuda, J. Ohta, An implantable CMOS image sensor with self-reset pixels for functional brain imaging, IEEE Trans. Electron Devices 63 (1) (2016) 215–222, https://doi.org/10.1109/TED.2015.2454435.

[13] J. Yuan, H.Y. Chan, S.W. Fung, B. Liu, An activity-triggered 95.3 db DR −75.6 db THD CMOS imaging sensor with digital calibration, IEEE J. Solid-State Circuits 44 (10) (2009) 2834–2843, https://doi.org/10.1109/JSSC.2009.2027929.

[14] A. Krishna, S. Rudresh, V. Shaw, H.R. Sabbella, C.S. Seelamantula, C.S. Thakur, Unlimited dynamic range analog-to-digital conversion, arXiv:1911.09371, 2019.
[15] A. Bhandari, F. Krahmer, R. Raskar, On unlimited sampling and reconstruction, IEEE Trans. Signal Process. 69 (2020) 3827–3839, https://doi.org/10.1109/TSP.2020.3041955.
[16] K. Itoh, Analysis of the phase unwrapping algorithm, Appl. Opt. 21 (14) (1982) 2470.
[17] E. Romanov, O. Ordentlich, Above the Nyquist rate, modulo folding does not hurt, IEEE Signal Process. Lett. 26 (8) (2019) 1167–1171, https://doi.org/10.1109/LSP.2019.2923835.
[18] L. Gan, H. Liu, High dynamic range sensing using multi-channel modulo samplers, in: Proc. Sensor Array and Multichannel Signal Process. Workshop (SAM), 2020, pp. 1–5.
[19] Y. Gong, L. Gan, H. Liu, Multi-channel modulo samplers constructed from Gaussian integers, IEEE Signal Process. Lett. 28 (2021) 1828–1832, https://doi.org/10.1109/LSP.2021.3108526.
[20] A. Bhandari, F. Krahmer, T. Poskitt, Unlimited sampling from theory to practice: Fourier-Prony recovery and prototype ADC, IEEE Trans. Signal Process. 70 (2022) 1131–1141.
[21] S. Rudresh, A. Adiga, B.A. Shenoy, C.S. Seelamantula, Wavelet-based reconstruction for unlimited sampling, in: Proc. IEEE Intl. Conf. Acoust., Speech and Signal Process. (ICASSP), 2018, pp. 4584–4588.
[22] A. Bhandari, F. Krahmer, R. Raskar, Unlimited sampling of sparse sinusoidal mixtures, in: Proc. Int. Symp. Info. Theory (ISIT), 2018, pp. 336–340.
[23] A. Bhandari, F. Krahmer, R. Raskar, Unlimited sampling of sparse signals, in: Proc. Intl. Conf. Acoust., Speech and Signal Process. (ICASSP), 2018, pp. 4569–4573.
[24] V. Bouis, F. Krahmer, A. Bhandari, Multidimensional unlimited sampling: a geometrical perspective, in: Proc. European Signal Process. Conf. (EUSIPCO), 2021, pp. 2314–2318.
[25] O. Musa, P. Jung, N. Goertz, Generalized approximate message passing for unlimited sampling of sparse signals, in: Proc. IEEE Global Conf. Signal and Info. Process. (GlobalSIP), 2018, pp. 336–340.
[26] D. Prasanna, C. Sriram, C.R. Murthy, On the identifiability of sparse vectors from modulo compressed sensing measurements, IEEE Signal Process. Lett. 28 (2021) 131–134, https://doi.org/10.1109/LSP.2020.3047584.
[27] S. Fernández-Menduiña, F. Krahmer, G. Leus, A. Bhandari, DoA estimation via unlimited sensing, in: Proc. European Signal Process. Conf. (EUSIPCO), 2021, pp. 1866–1870.
[28] A. Bhandari, M. Beckmann, F. Krahmer, The modulo Radon transform and its inversion, in: Proc. European Signal Process. Conf. (EUSIPCO), 2021, pp. 770–774.
[29] F. Ji Pratibha, W.P. Tay, Unlimited dynamic range signal recovery for folded graph signals, Signal Process. 198 (2022) 108574, https://doi.org/10.1016/j.sigpro.2022.108574.
[30] Y. Chen, A. Basu, L. Liu, X. Zou, R. Rajkumar, G.S. Dawe, M. Je, A digitally assisted, signal folding neural recording amplifier, IEEE Trans. Biomed. Circuits Syst. 8 (4) (2014) 528–542, https://doi.org/10.1109/TBCAS.2013.2288680.
[31] E. Romanov, O. Ordentlich, Spiked covariance estimation from modulo-reduced measurements, in: Int. Conf. Artificial Intelligence and Stats, PMLR, 2022, pp. 1298–1320.
[32] D. Florescu, A. Bhandari, Unlimited sampling via generalized thresholding, in: Int. Symp. Info. Theory (ISIT), 2022, pp. 1606–1611.
[33] D. Florescu, F. Krahmer, A. Bhandari, Unlimited sampling with hysteresis, in: Asilomar Conf. Signals, Sys., and Computers, 2021, pp. 831–835.
[34] D. Florescu, A. Bhandari, Unlimited sampling with local averages, in: Inte. Conf. Acoust., Speech and Signal Process. (ICASSP), 2022, pp. 5742–5746.
[35] S. Mulleti, E. Reznitskiy, N. Glazer, M. Namer, Y.C. Eldar, A hardware prototype of sub-Nyquist modulo sampling of FRI signals, in: Show and Tell Demo., IEEE Int. Conf. Acoust., Speech and Signal Process. (ICASSP), 2021.
[36] S. Mulleti, E. Azar, S.B. Shah, N. Glazer, S. Savariego, O. Cohen, E. Reznitskiy, M. Namer, Y.C. Eldar, Hardware demonstration of low-rate and high-dynamic range ADC, in: Show and Tell Demo., IEEE Int. Conf. Acoust., Speech and Signal Process. (ICASSP), 2022.
[37] Y.-M. Zhu, Generalized sampling theorem, IEEE Trans. Circuits Syst. II, Analog Digit. Signal Process. 39 (8) (1992) 587–588, https://doi.org/10.1109/82.168954.
[38] T.G. Dvorkind, Y.C. Eldar, E. Matusiak, Nonlinear and nonideal sampling: theory and methods, IEEE Trans. Signal Process. 56 (12) (2008) 5874–5890, https://doi.org/10.1109/TSP.2008.929872.
[39] E. Azar, S. Mulleti, Y.C. Eldar, Residual recovery algorithm for modulo sampling, in: Proc. Intl. Conf. Acoust., Speech and Signal Process. (ICASSP), 2022, pp. 5722–5726.
[40] S. Bubeck, et al., Convex optimization: algorithms and complexity, Found. Trends Mach. Learn. 8 (3–4) (2015) 231–357.
[41] M. Cucuringu, H. Tyagi, On denoising modulo 1 samples of a function, in: Int. Conf. Artificial Intelligence Statistics, 2018, pp. 1868–1876.
[42] M. Cucuringu, H. Tyagi, Provably robust estimation of modulo 1 samples of a smooth function with applications to phase unwrapping, J. Mach. Learn. Res. 21 (32) (2020).
[43] H. Tyagi, Error analysis for denoising smooth modulo signals on a graph, Appl. Comput. Harmon. Anal. 57 (2022) 151–184.
[44] M.J. Ablowitz, A.S. Fokas, Complex Variables: Introduction and Applications, 2nd edition, Cambridge Texts in Applied Mathematics, Cambridge University Press, 2003.
[45] A. Bhandari, F. Krahmer, On identifiability in unlimited sampling, in: Proc. Intl. Conf. Sampling Theory and Appl. (SampTA), 2019, pp. 1–4.
[46] A. Papoulis, Limits on bandlimited signals, Proc. IEEE 55 (10) (1967) 1677–1686.